JOURNAL OF THERMOPHYSICS AND HEAT TRANSFER
Vol. 14, No. 3, July–September 2000

Transient Analysis of Forced Convection Along a Wavy Surface in Micropolar Fluids

Cha'o-Kuang Chen* and Chi-Chang Wang†
National Cheng-Kung University, Tainan 701, Taiwan, Republic of China

Numerical results for transient laminar-forced convection along a wavy surface in micropolar fluids are presented. A simple coordinate transformation is employed to transform the complex wavy surface to a flat plate, and the obtained nonsimilarity boundary layer equation is solved numerically by the spline alternating-direction implicit method. The effects of micropolar parameter and wavy geometry on the velocity and temperature fields are examined. The transient skin friction and transient local and averaged heat-transfer rates decrease with time. Their axial distributions have a frequency equal to the frequency of the wavy surface, but their crests and troughs do not occur just at the crests and troughs of the wavy surface. The amplitudes of the transient local skin-friction coefficient and the transient local Nusselt number tend to increase as the wavy length and the wavy amplitude-wavelength ratio increases. Furthermore, the transient Nusselt number of a micropolar fluid is smaller than that of a Newtonian fluid everywhere, whereas the transient local skin-friction coefficient of a micropolar fluid is larger than that of a Newtonian fluid just near the leading edge.

Nomenclature

a = amplitude of wavy surface
B = dimensionless material parameter; Eq. (8)
C_f = skin-friction coefficient
C_p = specific heat of the fluid at constant pressure
h = heat-transfer coefficient
j = microinertia density
K_f = thermal conductivity
L = characteristic length
N = microrotation
Nu_m = total Nusselt number
Nu_x = local Nusselt number
Pr = Prandtl number; Eq. (8)
p = pressure
R = micropolar parameter; Eq. (8)
Re = generalized Reynolds number
$S(x)$ = surface geometry function
T = temperature
t = time
U_w = x component of the velocity of the inviscid flow, evaluated at the wavy surface
u = x component of velocity
v = y component of velocity
x, y = coordinates
α = wavy amplitude-wavelength ratio
γ = spin-gradient viscosity
θ = dimensionless temperature
κ = vortex viscosity
λ = dimensionless material parameter; Eq. (8)
μ = dynamic viscosity
ν_3 = microrotation component
ρ = density of fluid
σ = distance measured along the surface from the leading edge
τ = dimensionless time

Subscripts

w = wall surface
∞ = freestream condition

Superscripts

$-$ = dimensional variables
$\sim, \wedge$ = dimensionless quantity
$'$ = derivative with respect to x

Introduction

IN the past few decades microcontinuum fluid mechanics has received much attention. The theory of a micropolar fluid and thermomicropolar fluids, developed by Eringen,[1,2] can be used to explain the characteristics in certain fluids such as exotic lubricants, colloidal suspensions or polymeric fluids, liquid crystals and animal blood. The micropolar fluids exhibit certain microscopic effects arising from local structure and micromotion of the fluid elements. An excellent literature survey for micropolar fluid mechanics was provided by Ariman et al.[3,4]

Studies of the flows of heat convection in a micropolar fluid have focused mainly on flat plates[5–7] or regular surfaces[8,9] because the boundary condition is simple or the velocity of inviscid flow is easy to obtain. Few studies have been carried out to demonstrate the effects of complex geometry, such as irregular surfaces on forced convection. The prediction of heat transfer from irregular surfaces is a topic of fundamental importance, and it is often encountered in heat-transfer devices such as flat-plate solar collectors and flat-plate condensers in refrigerators. Using a transformation method, Yao[10] studied the natural-convection heat transfer from an isothermal vertical wavy surface. He obtained numerical results for a sinusoidal surface. His results showed that the local heat-transfer rate varies periodically along the wavy surface, with a frequency equal to twice the frequency of the surface. Recently, Chiu and Chou[11] studied the natural-convection heat transfer along a vertical wavy surface in micropolar fluids. The numerical results showed that as the micropolar parameter increases the heat-transfer rate decreases, while the hydrodynamic and thermal boundary-layer thicknesses and the skin-friction coefficient increase. The preceding literature survey shows that the transient forced convection along an irregular surface in micropolar fluids has not been studied so far.

The objective of this study is to analyze the transient forced convection flow in micropolar fluids along a vertical wavy surface by using Prandtl's transposition theorem and the spline alternating-direction method. Because the spline alternating-direction method can directly evaluate spatial derivatives without finite difference discretization, gradient boundary conditions are represented more accurately, and irregular boundaries are easier to analyze. The influence of micropolar parameter R and the wavy amplitude-wavelength

Received 19 August 1999; revision received 5 January 2000; accepted for publication 7 January 2000.

*Professor, Department of Mechanical Engineering.
†Postgraduate Student, Department of Mechanical Engineering.

ratio α on the transient local skin-friction coefficient and local Nusselt number are considered in this paper.

Mathematical Formulation

Consider the unsteady, laminar, incompressible, forced convection flow in a micropolar fluid over a semi-infinite wavy surface, having a cusped leading edge. The wavy surface is aligned parallel to a freestream of velocity U_∞, and the temperature of the wavy surfaces is held at a constant temperature T_w. The physical model and the coordinate system are shown in Fig. 1. In this work the profile of the surface is given by

$$\bar{y} = \bar{S}(\bar{x}) = \bar{a}\sin^2(\pi\bar{x}/L) \tag{1}$$

The governing equations with variable microinertia can be written as

$$\frac{\partial \bar{u}}{\partial \bar{x}} + \frac{\partial \bar{v}}{\partial \bar{y}} = 0 \tag{2}$$

$$\rho\left(\frac{\partial \bar{u}}{\partial t} + \bar{u}\frac{\partial \bar{u}}{\partial \bar{x}} + \bar{v}\frac{\partial \bar{u}}{\partial \bar{y}}\right) = -\frac{\partial \bar{p}}{\partial \bar{x}} + (\mu + \kappa)\left(\frac{\partial^2 \bar{u}}{\partial \bar{x}^2} + \frac{\partial^2 \bar{u}}{\partial \bar{y}^2}\right) + \kappa\frac{\partial v_3}{\partial \bar{y}} \tag{3}$$

$$\rho\left(\frac{\partial \bar{v}}{\partial t} + \bar{u}\frac{\partial \bar{v}}{\partial \bar{x}} + \bar{v}\frac{\partial \bar{v}}{\partial \bar{y}}\right) = -\frac{\partial \bar{p}}{\partial \bar{y}} + (\mu + \kappa)\left(\frac{\partial^2 \bar{v}}{\partial \bar{x}^2} + \frac{\partial^2 \bar{v}}{\partial \bar{y}^2}\right) + \kappa\left(-\frac{\partial v_3}{\partial \bar{x}}\right) \tag{4}$$

$$\rho j\left(\frac{\partial v_3}{\partial t} + \bar{u}\frac{\partial v_3}{\partial \bar{x}} + \bar{v}\frac{\partial v_3}{\partial \bar{y}}\right) = \kappa\left(\frac{\partial \bar{v}}{\partial \bar{x}} - \frac{\partial \bar{u}}{\partial \bar{y}} - 2v_3\right) + \gamma\left(\frac{\partial^2 v_3}{\partial \bar{x}^2} + \frac{\partial^2 v_3}{\partial \bar{y}^2}\right) \tag{5}$$

$$\rho C_p\left(\frac{\partial T}{\partial t} + \bar{u}\frac{\partial T}{\partial \bar{x}} + \bar{v}\frac{\partial T}{\partial \bar{y}}\right) = K_f\left(\frac{\partial^2 T}{\partial \bar{x}^2} + \frac{\partial^2 T}{\partial \bar{y}^2}\right) \tag{6}$$

The initial and appropriate boundary in conditions are

$\tau = 0$:

$$\theta(\bar{x}, \bar{y}, 0) = 0, \qquad \bar{u}(\bar{x}, \bar{y}, 0) = 0, \qquad v_3(\bar{x}, \bar{y}, 0) = 0 \tag{7a}$$

$\tau > 0$:

a) On the wavy surface $[\bar{y} = \bar{S}(\bar{x})]$:

$$T = T_w, \qquad \bar{u} = \bar{v} = 0 \tag{7b}$$

$$v_3 = 0 \tag{7c}$$

b) Matching with the quiescent freestream $(\bar{y} \to \infty)$:

$$T = T_\infty, \qquad \bar{u} = \bar{U}_w(\bar{x}), \qquad \bar{p} = \bar{p}_\infty(\bar{x}) \tag{7d}$$

$$v_3 = 0 \tag{7e}$$

where v_3 is the component of microrotation whose direction of rotation is in the $(x$–$y)$ plane; $\bar{U}_w(\bar{x})$ is the $\bar{x}$ component of the inviscid velocity at the surface $\bar{y} = \bar{S}(\bar{x})$. In Eq. (7c) the boundary condition for the microrotation at the fluid-solid interface is $v_3 = 0$, the condition of zero spin, as used by Takhar et al.[12]

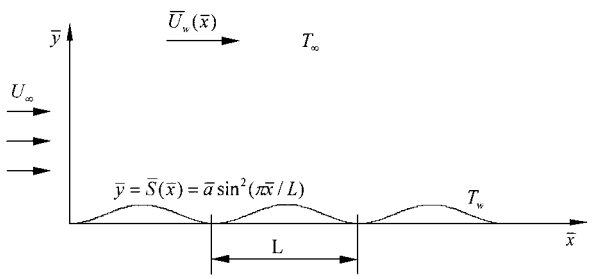

Fig. 1 Physical model.

The dimensionless variables are defined as

$$\tilde{x} = \frac{\bar{x}}{L}, \qquad \tilde{y} = \frac{\bar{y}}{L}, \qquad \tilde{\tau} = \frac{\bar{t}U_\infty}{L}, \qquad \alpha = \frac{\bar{a}}{L}$$

$$S(\tilde{x}) = \frac{\bar{S}(\bar{x})}{L}, \qquad \tilde{u} = \frac{\bar{u}}{U_\infty}, \qquad \tilde{v} = \frac{\bar{v}}{U_\infty}, \qquad \tilde{N} = \frac{v_3 L}{U_\infty}$$

$$\theta = \frac{T - T_\infty}{T_w - T_\infty}, \qquad U_w = \frac{\bar{U}_w}{U_\infty}, \qquad \tilde{p} = \frac{\bar{p}}{\rho U_\infty^2}, \qquad B = \frac{L\mu}{j\rho U_\infty}$$

$$\lambda = \frac{\gamma}{\mu j}, \qquad R = \frac{\kappa}{\mu}, \qquad Re = \frac{\rho U_\infty L}{\mu}, \qquad Pr = \frac{\mu C_p}{K_f} \tag{8}$$

Using the dimensionless variables defined in Eq. (8), Eqs. (2–6) become

$$\frac{\partial \tilde{u}}{\partial \tilde{x}} + \frac{\partial \tilde{v}}{\partial \tilde{y}} = 0 \tag{9}$$

$$\frac{\partial \tilde{u}}{\partial \tilde{\tau}} + \tilde{u}\frac{\partial \tilde{u}}{\partial \tilde{x}} + \tilde{v}\frac{\partial \tilde{u}}{\partial \tilde{y}} = -\frac{\partial \tilde{p}}{\partial \tilde{x}} + \frac{1 + R}{Re}\left(\frac{\partial^2 \tilde{u}}{\partial \tilde{x}^2} + \frac{\partial^2 \tilde{u}}{\partial \tilde{y}^2}\right) + \frac{R}{Re}\frac{\partial \tilde{N}}{\partial \tilde{y}} \tag{10a}$$

$$\frac{\partial \tilde{v}}{\partial \tilde{\tau}} + \tilde{u}\frac{\partial \tilde{v}}{\partial \tilde{x}} + \tilde{v}\frac{\partial \tilde{v}}{\partial \tilde{y}} = -\frac{\partial \tilde{p}}{\partial \tilde{y}} + \frac{1 + R}{Re}\left(\frac{\partial^2 \tilde{v}}{\partial \tilde{x}^2} + \frac{\partial^2 \tilde{v}}{\partial \tilde{y}^2}\right) + \frac{R}{Re}\left(-\frac{\partial \tilde{N}}{\partial \tilde{x}}\right) \tag{10b}$$

$$\frac{\partial \tilde{N}}{\partial \tilde{\tau}} + \tilde{u}\frac{\partial \tilde{N}}{\partial \tilde{x}} + \tilde{v}\frac{\partial \tilde{N}}{\partial \tilde{y}} = RB\left(\frac{\partial \tilde{v}}{\partial \tilde{x}} - \frac{\partial \tilde{u}}{\partial \tilde{y}} - 2\tilde{N}\right) + \frac{\lambda}{Re}\left(\frac{\partial^2 \tilde{N}}{\partial \tilde{x}^2} + \frac{\partial^2 \tilde{N}}{\partial \tilde{y}^2}\right) \tag{11}$$

$$\frac{\partial \theta}{\partial \tilde{\tau}} + \tilde{u}\frac{\partial \theta}{\partial \tilde{x}} + \tilde{v}\frac{\partial \theta}{\partial \tilde{y}} = \frac{1}{RePr}\left(\frac{\partial^2 \theta}{\partial \tilde{x}^2} + \frac{\partial^2 \theta}{\partial \tilde{y}^2}\right) \tag{12}$$

Using Prandtl's transposition theorem to transform the irregular wavy surface into a flat surface as extended by Yao[13] and letting $Re \to \infty$ (boundary-layer approximation), the preceding equations can be written as

$$\frac{\partial \hat{u}}{\partial \hat{x}} + \frac{\partial \hat{v}}{\partial \hat{y}} = 0 \tag{13}$$

$$\frac{\partial \hat{u}}{\partial \hat{\tau}} + \hat{u}\frac{\partial \hat{u}}{\partial \hat{x}} + \hat{v}\frac{\partial \hat{u}}{\partial \hat{y}} = -\frac{\partial \hat{p}}{\partial \hat{x}} + Re^{\frac{1}{2}}S'\frac{\partial \hat{p}}{\partial \hat{y}} + (1 + R)(1 + S'^2)\frac{\partial^2 \hat{u}}{\partial \hat{y}^2} + R\frac{\partial \hat{N}}{\partial \hat{y}} \tag{14a}$$

$$\hat{u}^2 S'' + S'\frac{Gr}{Re^2}\theta = S'\frac{\partial \hat{p}}{\partial \hat{x}} - Re^{\frac{1}{2}}(1 + S'^2)\frac{\partial \hat{p}}{\partial \hat{y}} \tag{14b}$$

$$\frac{\partial \hat{N}}{\partial \hat{\tau}} + \hat{u}\frac{\partial \hat{N}}{\partial \hat{x}} + \hat{v}\frac{\partial \hat{N}}{\partial \hat{y}} = RB\left(-(1 + S'^2)\frac{\partial \hat{u}}{\partial \hat{y}} - 2\hat{N}\right) + \lambda(1 + S'^2)\frac{\partial^2 \hat{N}}{\partial \hat{y}^2} \tag{15}$$

$$\frac{\partial \theta}{\partial \hat{\tau}} + \hat{u}\frac{\partial \theta}{\partial \hat{x}} + \hat{v}\frac{\partial \theta}{\partial \hat{y}} = \frac{1}{Pr}(1 + S'^2)\frac{\partial^2 \theta}{\partial \hat{y}^2} \tag{16}$$

where

$$\hat{x} = \tilde{x}, \qquad \hat{y} = [\tilde{y} - S(\tilde{x})]Re^{\frac{1}{2}}, \qquad \hat{\tau} = \tilde{\tau}, \qquad \hat{u} = \tilde{u}$$

$$\hat{v} = (\tilde{v} - S'\tilde{u})Re^{\frac{1}{2}}, \qquad \hat{N} = \tilde{N}Re^{-\frac{1}{2}}, \qquad \hat{p} = \tilde{p} - \tilde{p}_\infty \quad (17)$$

Equation (14b) indicates that the pressure gradient along the y direction is $\mathcal{O}(Re^{-1/2})$. This implies that the lowest-order pressure gradient along the x direction can be determined from the inviscid flow solution and is given by

$$\frac{\partial \hat{p}}{\partial \hat{x}} = -\left[(1 + S'^2)U_w U_w' + S'S''U_w^2\right] \quad (18)$$

Eliminating $\partial \hat{p}/\partial \hat{y}$ between Eqs. (14a) and (14b) and using Eq. (18) gives

$$\frac{\partial \hat{u}}{\partial \hat{\tau}} + \hat{u}\frac{\partial \hat{u}}{\partial \hat{x}} + \hat{v}\frac{\partial \hat{u}}{\partial \hat{y}} = \frac{1}{1 + S'^2}\left(-\frac{\partial \hat{p}}{\partial \hat{x}} - S'S''\hat{u}^2\right)$$

$$+ (1 + R)(1 + S'^2)\frac{\partial^2 \hat{u}}{\partial \hat{y}^2} + R\frac{\partial N}{\partial \hat{y}} \quad (19)$$

Here we define the dimensionless variables

$$x = \hat{x}, \qquad y = \hat{y}\left(\frac{2\hat{x}}{U_w}\right)^{-\frac{1}{2}}, \qquad \tau = \hat{\tau}\left(\frac{2\hat{x}}{U_w}\right)^{-1}$$

$$u = \frac{\hat{u}}{U_w}, \qquad v = \hat{v}\left(\frac{2\hat{x}}{U_w}\right)^{\frac{1}{2}}, \qquad N = \hat{N}\left(\frac{2\hat{x}}{U_w}\right)^{\frac{1}{2}} \quad (20)$$

Equations (13), (15), (16), and (19) can be further transformed by using the preceding dimensionless variables. The equations obtained are

$$2x\frac{\partial u}{\partial x} - y\left(1 - x\frac{U_w'}{U_w}\right)\frac{\partial u}{\partial y} + \frac{\partial v}{\partial y} + 2x\frac{U_w'}{U_w}u = 0 \quad (21)$$

$$\frac{\partial u}{\partial \tau} + 2xu\frac{\partial u}{\partial x} + \left(v - yu\left(1 - x\frac{U_w'}{U_w}\right)\right)\frac{\partial u}{\partial y}$$

$$+ 2x(u^2 - 1)\left(\frac{S'S''}{1 + S'^2} + \frac{U_w'}{U_w}\right)$$

$$= (1 + R)(1 + S'^2)\frac{\partial^2 u}{\partial y^2} + \frac{R}{U_w}\frac{\partial N}{\partial y} \quad (22)$$

$$\frac{\partial N}{\partial \tau} + 2xu\frac{\partial N}{\partial x} + \left(v - yu\left(1 - x\frac{U_w'}{U_w}\right)\right)\frac{\partial N}{\partial y} - uN\left(1 - x\frac{U_w'}{U_w}\right)$$

$$= xRB\left(-2(1 + S'^2)\frac{\partial u}{\partial y} - 4\frac{N}{U_w}\right) + \lambda(1 + S'^2)\frac{\partial^2 N}{\partial y^2} \quad (23)$$

$$\frac{\partial \theta}{\partial \tau} + 2xu\frac{\partial \theta}{\partial x} + \left(v - yu\left(1 - x\frac{U_w'}{U_w}\right)\right)\frac{\partial \theta}{\partial y} = \frac{1 + S'^2}{Pr}\frac{\partial^2 \theta}{\partial y^2} \quad (24)$$

The corresponding boundary conditions become

$t = 0$:

$$\theta(x, y, 0) = 0, \qquad u(x, y, 0) = 0, \qquad N(x, y, 0) = 0$$

$t > 0$:

$$y = 0: \quad \theta = 1, \quad u = v = N = 0$$

$$y \to \infty: \quad \theta = 0, \quad u = 1, \quad N = 0 \quad (25)$$

Moreover, we would examine the inviscid flow along the wavy surface. The inviscid solution obtained here is valid only for small values of the amplitude-wavelength ratio. The potential-flow solution $U_w(x)$ for small values of $\alpha(\ll 1)$ is[14]

$$U_w(x) = 1 + \frac{1}{\pi}\int_0^\infty \frac{S'(t)}{x - t}\,dt + \mathcal{O}(\alpha^2) \quad (26)$$

The singular point in this integral can be removed by using the residue theorem, and it can be expressed as

$$U_w(x) = 1 + \alpha\left(-\pi\cos(2\pi x) + \int_0^\infty \frac{\sin(2\pi t)}{x + t}\,dt\right) + \mathcal{O}(\alpha^2) \quad (27)$$

An important physical quantity is the skin-friction coefficient defined as

$$C_f = 2\tau_w \Big| \rho U_w^2 \quad (28a)$$

where the shearing stress on the surface is given by

$$\tau_w = \left(\mu\left(\frac{\partial \bar{u}}{\partial \bar{y}} + \frac{\partial \bar{v}}{\partial \bar{x}}\right) + \kappa\left(\frac{\partial \bar{u}}{\partial \bar{y}} + v_3\right)\right)_{\bar{y} = \bar{S}(\bar{x})} \quad (28b)$$

Using Eqs. (28a) and (28b), we obtain

$$(2Re_{\bar{x}})^{\frac{1}{2}}C_f = (2 + R)U_w^{\frac{3}{2}}(1 - S'^2)\frac{\partial u}{\partial y} \quad (28c)$$

The local Nusselt number is defined as

$$Nu_{\bar{x}} = \frac{h_{\bar{x}}\bar{x}}{K_f} = \frac{-(\partial T/\partial n)\bar{x}}{T_w - T_\infty} \quad (29a)$$

where $\partial T/\partial n$ represents differentiation along the normal to the surface:

$$\frac{\partial T}{\partial n} = \sqrt{\left(\frac{\partial T}{\partial \bar{x}}\right)^2 + \left(\frac{\partial T}{\partial \bar{y}}\right)^2} \quad (29b)$$

Using Eqs. (29a) and (29b), we obtain

$$\left(\frac{2}{Re_{\bar{x}}}\right)^{\frac{1}{2}}Nu_{\bar{x}} = -\left[(1 + S'^2)U_w\right]^{\frac{1}{2}}\frac{\partial \theta}{\partial y}\bigg|_{y=0} \quad (29c)$$

The total Nusselt number is obtained by averaging the heat transfer over the surface from the leading edge to $\sigma(x)$. It is given by

$$Nu_m = h_m\sigma(\bar{x})/K_f \quad (30a)$$

where

$$h_m = q_m/(T_w - T_\infty) \quad (30b)$$

$$q_m = \frac{1}{\sigma}\int_0^\sigma -K_f\frac{\partial T}{\partial n}\,d\sigma \quad (30c)$$

$$\sigma = \int_0^x (1 + S'^2)^{\frac{1}{2}}\,dx \quad (30d)$$

The variation of $(2/Re_{\bar{x}})^{1/2}Nu_m$ can be obtained by integration of the preceding equation. It is expressed as

$$\left(\frac{2}{Re_{\bar{x}}}\right)^{\frac{1}{2}}Nu_m = -\left(\frac{2}{x}\right)^{\frac{1}{2}}\int_0^x \left(\frac{U_w}{2x}\right)^{\frac{1}{2}}(1 + S'^2)\frac{\partial \theta}{\partial y}\bigg|_{y=0}\,dx \quad (30e)$$

Numerical Method

The spline alternating-direction implicit method (SADI), an improved version of the cubic spline collocation method,[15] was used to perform the numerical computation by Char and Chen[16] and Wang and Kahawita.[17] Equations (21–24) can be discretized as

$$2x_i\left(\frac{\partial u}{\partial x}\right)_{i,j}^{n+1} - y_j\left(1 - x_i\frac{U_w'}{U_w}\right)l_u^{n+1} + \left(\frac{\partial v}{\partial y}\right)_{i,j}^{n+1} + 2x_i u_{i,j}^{n+1}\frac{U_w'}{U_w} = 0 \tag{31}$$

$$\frac{u_{i,j}^{n+1} - u_{i,j}^{n}}{\Delta\tau} + 2x_i u_{i,j}^{n+1}\left(\frac{\partial u}{\partial x}\right)_{i,j}^{n+1} + \left(v_{i,j}^{n+1} - y_j u_{i,j}^{n+1}\left(1 - x_i\frac{U_w'}{U_w}\right)\right)l_u^{n+1} + 2x_i\left[\left(u_{i,j}^{n+1}\right)^2 - 1\right] \times \left(\frac{S'S''}{1+S'^2} + \frac{U_w'}{U_w}\right) = (1+R)(1+S'^2)L_u^{n+1} + \frac{R}{U_w}l_N^{n+1} \tag{32}$$

$$\frac{N_{i,j}^{n+1} - N_{i,j}^{n}}{\Delta\tau} + 2x_i u_{i,j}^{n+1}\left(\frac{\partial N}{\partial x}\right)_{i,j}^{n+1} + \left(v_{i,j}^{n+1} - y_j u_{i,j}^{n+1}\left(1 - x_i\frac{U_w'}{U_w}\right)\right)l_N^{n+1} - u_{i,j}^{n+1}N_{i,j}^{n+1}\left(1 - x_i\frac{U_w'}{U_w}\right) = BRx_i\left(-2(1+S'^2) - l_u^{n} - 4\frac{N_{i,j}^{n+1}}{U_w}\right) + \lambda(1+S'^2)l_N^{n+1} \tag{33}$$

$$\frac{\theta_{i,j}^{n+1} - \theta_{i,j}^{n}}{\Delta\tau} + 2x_i u_{i,j}^{n+1}\left(\frac{\partial\theta}{\partial x}\right)_{i,j}^{n+1} + \left(v_{i,j}^{n+1} - y_j u_{i,j}^{n+1}\left(1 - x_i\frac{U_w'}{U_w}\right)\right)l_\theta^{n+1} = \frac{1+S'^2}{Pr}l_\theta^{n+1} \tag{34}$$

where

$$\Delta x = x_i - x_{i-1}, \qquad \Delta y = y_i - y_{i-1}$$

$$\left(\frac{\partial\phi}{\partial x}\right)_{i,j} = \frac{\phi_{i,j} - \phi_{i,j-1}}{\Delta x_i} \quad \text{for} \quad i = 1$$

$$\left(\frac{\partial\phi}{\partial x}\right)_{i,j} = \frac{-3\phi_{i,j} + 4\phi_{i,j-1} - \phi_{i,j-2}}{2\Delta x_i} \quad \text{for} \quad i \geq 2$$

$$l_\phi = \frac{\partial\phi}{\partial y}, \qquad L_\phi = \frac{\partial^2\phi}{\partial y^2} \tag{35}$$

where ϕ refers to u, N, and θ, and the quantity $\Delta\tau = \tau^{n+1} - \tau^n$ represents the time step.

The SADI procedure was applied to perform the numerical computation. Using the spline formulation, the forced convection boundary-layer equations of Eqs. (31–34) are written in the following form:

$$\phi_{i,j}^{n+1} = F_{i,j} + G_{i,j}l_{\phi_{i,j}}^{n+1} + S_{i,j}L_{\phi_{i,j}}^{n+1} \tag{36}$$

The quantities F, G, and S are known coefficients evaluated at previous time steps. For u:

$$F_{i,j} = u_{i,j}^{n} + \Delta\tau\left\{-2xu_{i,j}^{n+1}\left(\frac{\partial u}{\partial x}\right)^{n+1} - 2x\left[\left(u_{i,j}^{n+1}\right)^2 - 1\right]\left(\frac{S'S''}{1+S'^2} + \frac{U_w'}{U_w}\right) + \frac{R}{U_w}l_N^{n+1}\right\}$$

$$G_{i,j} = -\Delta\tau\left(v_{i,j}^{n+1} - y_i u_{i,j}^{n+1}\left(1 - x\frac{U_w'}{U_w}\right)\right)$$

$$S_{i,j} = \Delta\tau(1+R)(1+S'^2)$$

For N:

$$F_{i,j} = N_{i,j}^{n} + \Delta\tau\left\{-2xu_{i,j}^{n+1}\left(\frac{\partial N}{\partial x}\right)^{n+1} + \left(1 - x\frac{U_w'}{U_w}\right)u_{i,j}^{n+1} + RBx\left(-2(1+S'^2)l_u^{n+1} - 4\frac{N^{n+1}}{U_w}\right)\right\}$$

$$G_{i,j} = -\Delta\tau\left(v_{i,j}^{n+1} - y_i u_{i,j}^{n+1}\left(1 - x\frac{U_w'}{U_w}\right)\right)$$

$$S_{i,j} = \Delta\tau\lambda(1+S'^2)$$

For θ:

$$F_{i,j} = \theta_{i,j}^{n} + \Delta\tau\left[-2xu_{i,j}^{n+1}\left(\frac{\partial\theta}{\partial x}\right)^{n+1}\right]$$

$$G_{i,j} = -\Delta\tau\left(v_{i,j}^{n+1} - y_i u_{i,j}^{n+1}\left(1 - x\frac{U_w'}{U_w}\right)\right)$$

$$S_{i,j} = \frac{\Delta\tau}{Pr}(1+S'^2)$$

Equation (36) is of a general nature, independent of the method used for the spatial integration.

By using the cubic spline relations described in Ref. 15, Eq. (36) can be written in the following tridiagonal form:

$$A_{i,j}\phi_{i,j-1} + B_{i,j}\phi_{i,j} + C_{i,j}\phi_{i,j+1} = D_{i,j} \tag{37}$$

Equation (37) can be easily solved by using the Thomas algorithm.

The numerical procedure is described as follows:

1) Set suitable boundary conditions and initial values.

2) Calculate the transient solution at every x station iteratively marching from the leading edge ($x = 0$). The convergence criterion is

$$\left|\frac{\phi_{i,j}^{z+1} - \phi_{i,j}^{z}}{\phi_{i,j}^{z+1}}\right| \leq 1 \times 10^{-5} \tag{38}$$

where ϕ refers to θ, u, v, or N and z denotes the number of iterations.

3) Return to step 2) and proceed with the calculation for the next time step ($\tau + \Delta\tau$) until the solution between two successive time steps ceases to change significantly, i.e.,

$$\left|\frac{\phi_{i,j}^{n+1} - \phi_{i,j}^{n}}{\phi_{\max}^{n+1}}\right| < 1 \times 10^{-6} \tag{39}$$

where n denotes the number of time steps.

Results and Discussion

An accuracy test of grid fineness is made for the arrangements of 100×20, 100×50, 100×150, 25×50, 50×50, and 100×50.

Table 1 Local heat-transfer rate $(2/Re_{\bar{x}})^{1/2}Nu_{\bar{x}}$ and skin-friction coefficient $(2Re_{\bar{x}})^{1/2}C_f$: a) for different grid sizes, b) for different time steps, and c) compared to theoretical solution

	$(2/Re_{\bar{x}})^{1/2}Nu_{\bar{x}}$		$(2Re_{\bar{x}})^{1/2}C_f$	
Parameter	x = 0.16	x = 4	x = 0.16	x = 4
a) Steady-state solutions: Pr = 0.73, α = 0.002, R = 1, B = 1, λ = 5, x ∈ [0, 4], and y ∈ [0, 10]				
100 × 20	0.393842	0.379809	1.131646	0.968401
100 × 50	0.394535	0.376537	1.131432	0.960356
100 × 150	0.394248	0.375848	1.129922	0.958338
25 × 50	0.394550	0.377982	1.132669	0.959618
50 × 50	0.394376	0.375799	1.130772	0.956972
100 × 50	0.394393	0.376083	1.130753	0.959037
100 × 75[a]	0.391625	0.378118	1.123619	0.960467
100 × 200[a]	0.393746	0.376413	1.127222	0.959405
b) Transient-state solution: grid sizes = 50 × 50, τ = 1				
Δτ = 0.001	0.555847	0.53622	1.559476	1.46801
Δτ = 0.005	0.555732	0.52747	1.560010	1.46861
Δτ = 0.010	0.554803	0.496616	1.528782	1.469809
c) Present solutions: α = 0, R = 0, grid sizes 4 = 50 × 50				
Pr = 1.00	0.469726	0.469653	0.939451	0.939306
	(0.469519)[b]		(0.939083)[b]	
Pr = 0.73	0.420412	0.420198	0.939745	0.939306
	(0.4227601)[b]		(0.939083)[b]	

[a]Uniform grid (y direction). [b]Parenthetical values are obtained from Eqs. (40a) and (40b).

Table 2 Values of parameters in this study

Parameter	Value
Pr	1.0
B	1.0
λ	5.0
α	0.002, 0.005
R	0, 1.0, 5.0

The time interval is taken as $\Delta\tau = 0.001$, 0.005, and 0.01. The time step and grid dependence of the solutions have been tested and shown in Table 1. The difference between the results for grids of 50×50 and 100×50 are less than 0.1% in the local Nusselt number and the skin-friction coefficient at $Pr = 0.73$, $\alpha = 0.002$, $R = 1$, $B = 1$, $\lambda = 5$, $x \in [0, 4]$, and $y \in [0, 10]$. The difference between the results for $\Delta\tau = 0.005$ and 0.001 are less than 0.2% in the transient local Nusselt number and skin-friction coefficient for the spatial grid of 50×50. Thus, 50×50 nonuniform grid with a smaller spacing mesh points in the neighborhood of the fluid-solid boundary at y direction and the time interval $\Delta\tau = 0.005$ are used in the present work. To verify the accuracy of the computer program used in this study, the results obtained for Newtonian fluids (i.e., $R = 0$) over a flat plate (i.e., $\alpha = 0$) are computed at $Pr = 1$ and 0.73. The skin-friction coefficient and local Nusselt number values are in good agreement with results obtained by the following equations:

$$Nu_{\bar{x}} = 0.332\, Re_{\bar{x}}^{\frac{1}{2}} Pr^{\frac{1}{3}} \tag{40a}$$

$$C_f = 0.664 \left| Re_{\bar{x}}^{\frac{1}{2}} \right. \tag{40b}$$

Numerical results have been obtained for the surface described by $S(\bar{x}) = \bar{a}\sin^2(\pi\bar{x}/L)$, or $S(x) = \alpha\sin^2(\pi x)$, for amplitude-wavelength ratios $\alpha = 0.002$ and 0.005. Three values of micropolar parameter (i.e., $R = 0$, 1, and 5) are used. The material parameter $B = 1$, Prandtl number $Pr = 1$, and material parameter $\lambda = 5$ are taken throughout the study. Details of the variable parameters are presented in Table 2.

Before solving the dimensionless governing differential equations (21–24) subject to the relevant boundary conditions in Eq. (25), the Simpson's integral rule has been used to compute the value of $U_w(x)$ in Eq. (27). Figure 2 shows the axial distributions of the inviscid surface velocity $U_w(x)$ and the pressure gradient dp/dx for $\alpha = 0.002$ and 0.005. The inviscid surface velocity varies periodically along the surface with a cycle equal to that of the wavy surface. The flow accelerates along the portion of the surface from trough to crest, where the slope S' is positive, while it decelerates along the portion of the surface from crest to trough, where the slope S' is negative. The pressure gradient distribution has a frequency equal to that of the wavy surface. The pressure gradient dp/dx is negative in regions where the inviscid flow accelerates, and it becomes positive in regions where the inviscid flow decelerates. The maximum and minimum values of the pressure gradient occur at the points of inflection of the wavy surface. The pressure gradient tends to increase as the amplitude-wavelength ratio is increased. From the potential flow theory it is evident that the pressure gradient at the leading edge ($x = 0$) is infinite because of the sudden change in curvature at that point.

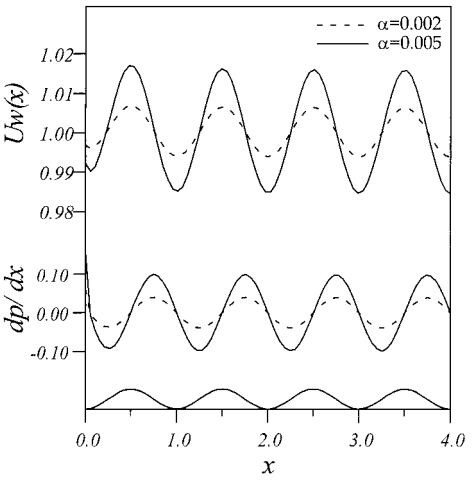

Fig. 2 Inviscid surface velocity distribution and axial distribution of d*p*/d*x*.

Figures 3 and 4 display the results for the distribution of the transient axial velocity component u, temperature θ for Newtonian fluid (i.e., $R = 0$) at the $x = 1.75$ (node). Figure 3 illustrates that the axial velocity component tends to decrease with increasing amplitude-wavelength ratio. The temperature increases with the amplitude-wavelength ratio as shown in Fig. 4; the smaller the axial velocity, the smaller the heat-transfer rate. Because the temperature of the wavy surface is kept constant, the temperature profile becomes higher as the amplitude-wavelength ratio is increased. As the time increases,

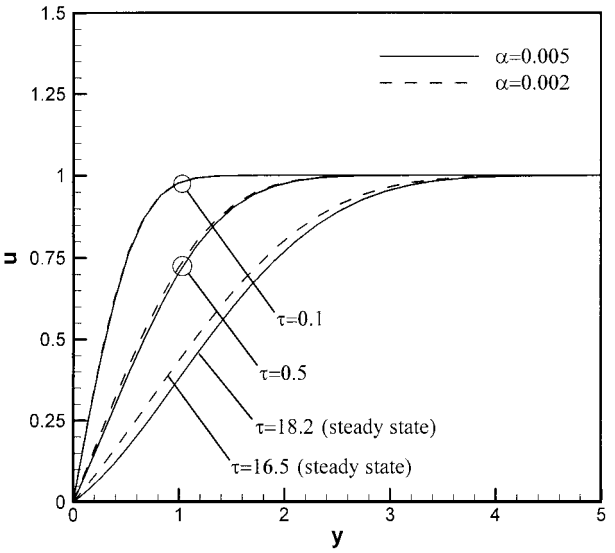

Fig. 3 Transient axial velocity profiles for Newtonian fluids (i.e., $R = 0$) at $x = 1.75$.

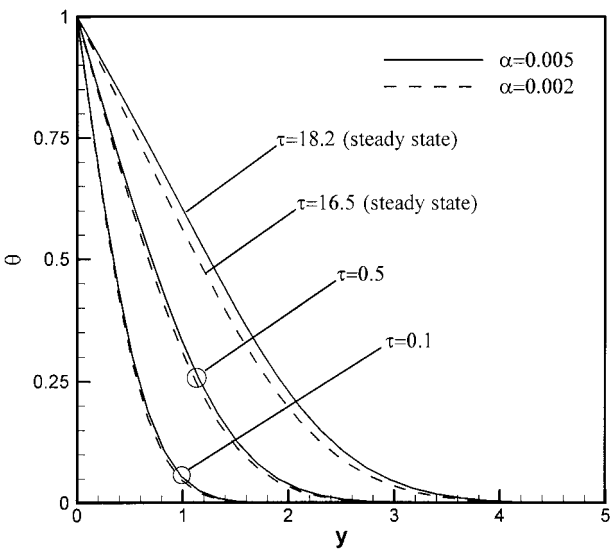

Fig. 4 Transient temperature distribution for Newtonian fluids (i.e., $R = 0$) at $x = 1.75$.

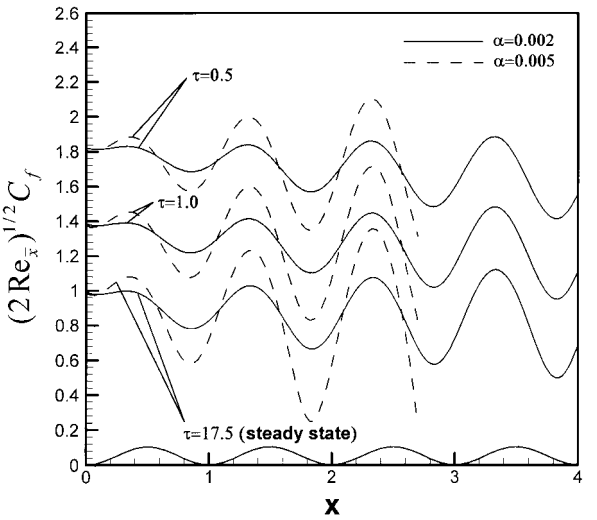

Fig. 5 Transient axial distribution of $(2Re_{\bar{x}})^{1/2}C_f$ for $R = 1, \lambda = 5, B = 1$, and $Pr = 1$.

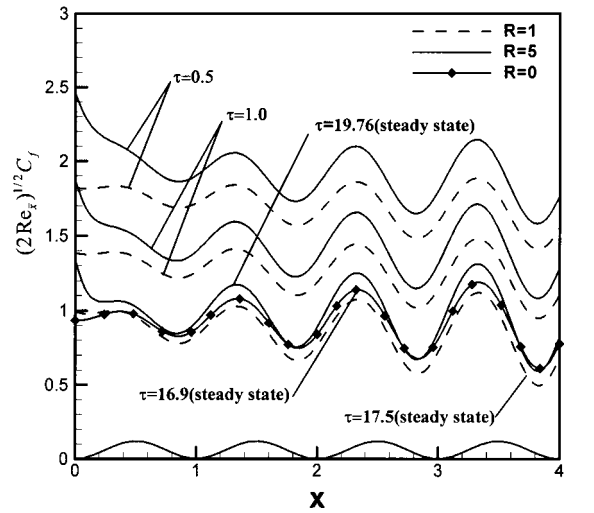

Fig. 6 Transient axial distribution of $(2Re_{\bar{x}})^{1/2}C_f$ for $\alpha = 0.002$, $\lambda = 5$, $B = 1$, and $Pr = 1$.

the axial velocity decreases but the temperature increases. However, the hydrodynamic and thermal boundary-layer thicknesses increase progressively with the time.

Figure 5 shows the variation of the transient skin-friction coefficient $(2Re_{\bar{x}})^{1/2}C_f$ with $R = 1$, $\lambda = 5$, $B = 1$, including the limiting case of a steady-state condition ($\tau = 17.5$) $Pr = 1$ for $\alpha = 0.002$ and 0.005, for comparison. As time increases, the hydrodynamic boundary-layer thickness increases, thus decreasing the transient skin-friction coefficient at the same x position. The curves show a periodic variation with a frequency equal to the frequency of the wavy surface under both the transient and steady-state conditions.

In Fig. 5 it can be seen that the skin-friction coefficient $(2Re_{\bar{x}})^{1/2}C_f$ becomes negative and the numerical solution becomes unstable at $\tau > 0.5$ near $x = 2.85$ for $\alpha = 0.005$ and $R = 1$. The results can be explained as follows. The numerical solution become unstable at some values of x and α. This occurs at a large value of x when α is small, or at a small value of x when α is large. The negative value of the transient local skin-friction coefficient $(2Re_{\bar{x}})^{1/2}C_f$ indicates that the flow is reversed. We do not present the numerical results beyond this point because the boundary-layer theory is meaningless thereafter. Therefore, this work presents the results for x ranging from 0 to 2.7 when wavy amplitude-wavelength ratio $\alpha = 0.005$.

Figure 6 shows the transient axial distribution of $(2Re_{\bar{x}})^{1/2}C_f$ with $\alpha = 0.002$, $\lambda = 5$, $B = 1$, and $Pr = 1$ for the micropolar parameter $R = 0$, 1, and 5. The local skin-friction coefficient at the leading edge ($x = 0$) increases with the vortex viscosity parameter R, as shown in Fig. 6. The local skin-friction coefficient for micropolar fluids tends to decrease rapidly near the leading edge as the fluid moves downstream, which is different from the behavior for Newtonian fluids. Moreover, Fig. 6 shows that the transient local skin-friction coefficient increases with the micropolar parameter R for a micropolar fluid. This phenomenon reflects the fact that increasing the value of micropolar parameter R results in an enhancement of the total viscosity in fluid flow, thus increasing the skin friction. In addition, whereas the values of the wavy length x and the wavy amplitude-wavelength ratio α increase, the amplitude of the axial distribution of $(2Re_{\bar{x}})^{1/2}C_f$ increases, as shown in Figs. 5 and 6. The curve for the transient axial distribution of $(2Re_{\bar{x}})^{1/2}C_f$, as shown in Figs. 5 and 6, shows a frequency equal to the frequency of the wavy surface. However, the crests and troughs of the transient local skin-friction coefficient are shifted slightly upstream of the crests and troughs of the wavy surface. For a complete cycle ($1 < x < 2$) the maximum value occurs at $x = 1.35$ but not at $x = 1.5$ (crest), and the minimum value occurs at $x = 1.85$ but not at $x = 2$ (trough).

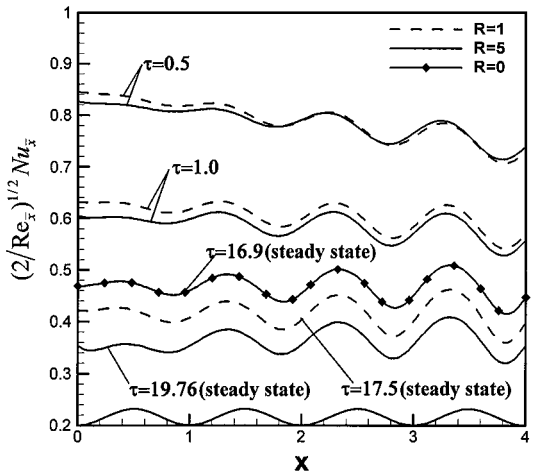

Fig. 7 Transient axial distribution of $(2/Re_{\bar{x}})^{1/2}Nu_{\bar{x}}$ for $\alpha = 0.002$, $\lambda = 5$, $B = 1$, and $Pr = 1$.

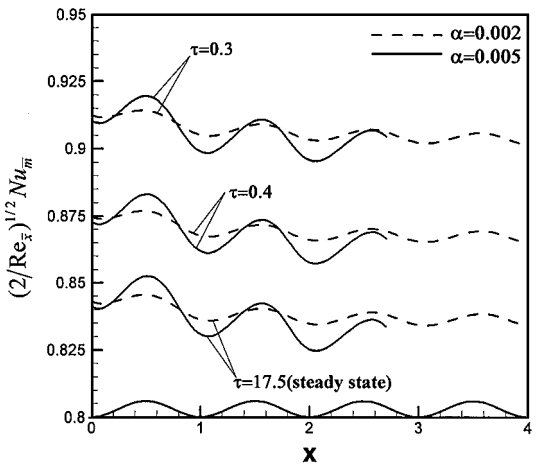

Fig. 8 Transient axial distribution of $(2/Re_{\bar{x}})^{1/2}Nu_m$ for $R = 1$, $\lambda = 5$, $B = 1$, and $Pr = 1$.

The transient axial distribution of $(2/Re_{\bar{x}})^{1/2}Nu_{\bar{x}}$ with $\alpha = 0.002$, $\lambda = 5$, $B = 1$, $Pr = 1$ for two different values of the micropolar parameter R is shown in Fig. 7. It is observed that the value of $(2/Re_{\bar{x}})^{1/2}Nu_{\bar{x}}$ decreases progressively with time and that the decreasing rate increases with increasing micropolar parameter R. However, Fig. 5 shows that the decreasing rate for the skin-friction coefficient $(2Re_{\bar{x}})^{1/2}C_f$ is equal for different wavy amplitude-wavelength ratios ($\alpha = 0.002$ and 0.005) with the same micropolar parameter $R = 1$. Moreover, a micropolar fluid with large micropolar parameters R has low transient Nusselt numbers. This phenomenon reflects the fact that increasing the value of vortex viscosity results in an enhancement of the total viscosity in fluid flow, decreasing both the velocity and the heat-transfer rate while increasing skin coefficient. The curve for $\alpha = 0.002$ and 0.005 exhibits the same periodic behavior as in Figs. 5 and 6, with a frequency equal to the frequency of the wavy surface. However, the crests and troughs of the transient local Nusselt number are shifted slightly upstream of the crests and troughs of the wavy surface.

Figure 8 shows the transient axial distribution of $(2/Re_{\bar{x}})^{1/2}Nu_m$ for $R = 1$, $\lambda = 5$, $B = 1$, $Pr = 1$, where the transient total Nusselt number Nu_m is obtained by averaging the heat transfer over the surface from the leading edge to $\sigma(x)$; Eq. (30e). The value of $(2/Re_{\bar{x}})^{1/2}Nu_m$ decreases progressively with time. Figure 8 shows that the peaks of the total heat-transfer rate occur near the peaks of the wavy surface, where the inviscid freestream velocity is maximum as shown in Fig. 2, but they are shifted slightly downstream of the crests of the wavy surface. This is different from the results

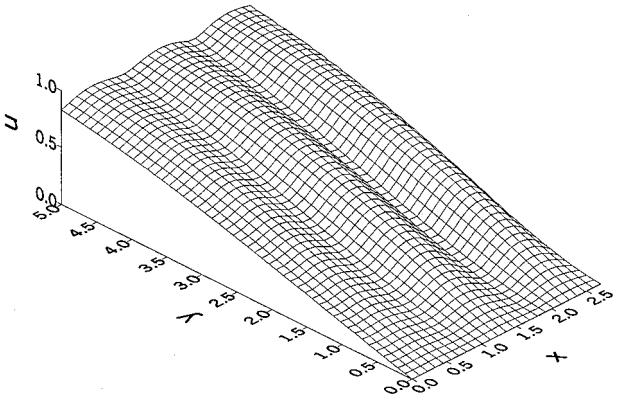

Fig. 9 Axial velocity profiles of u ($\tau = 20$, $\alpha = 0.005$, $R = 5$, $\lambda = 5$, and $B = 1$).

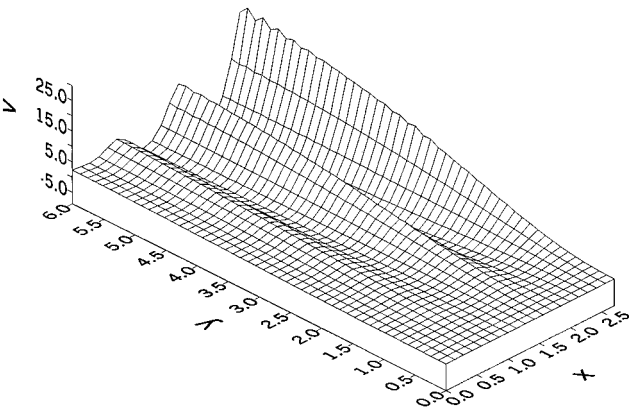

Fig. 10 Normal velocity profiles of v ($\tau = 20$, $\alpha = 0.005$, $R = 5$, $\lambda = 5$, and $B = 1$).

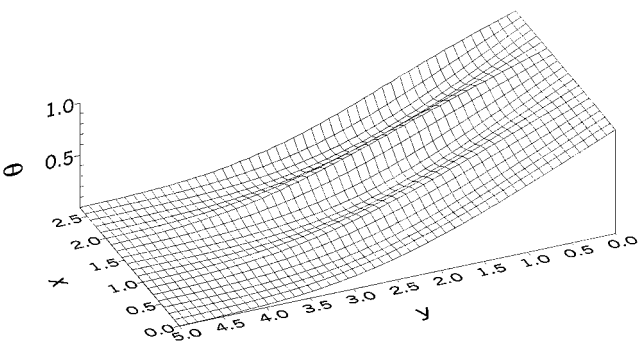

Fig. 11 Temperature profiles of θ ($\tau = 20$, $\alpha = 0.005$, $R = 5$, $\lambda = 5$, and $B = 1$).

for the transient local skin-friction coefficient and the transient local Nusselt number shown in Figs. 5, 6, and 7, respectively. The amplitude of the total Nusselt number $(2/Re_{\bar{x}})^{1/2}Nu_m$ decreases as the wavy length x increases or the wavy amplitude α decreases. Therefore, the wavy variation of the total Nusselt number can only be observed near the leading edge, or at a large value of the wave amplitude-wavelength ratio.

Figures 9, 10, 11, and 12 show the three-dimensional plot of the axial velocity component u, normal velocity component v, temperature θ, and microrotation N, respectively, for $\tau = 20$, $B = 1$, $\lambda = 5$, $R = 5.0$, and $\alpha = 0.005$. The variation rate and boundary layer of the axial velocity component u, temperature θ, and microrotation N are almost constant far downstream of the leading edge. In addition, as far away from the wavy surface (i.e., $y \to \infty$), the magnitude of $\partial u/\partial x$ and $\partial u/\partial y$ approach to zero in Fig. 9. Thus, it is seen from

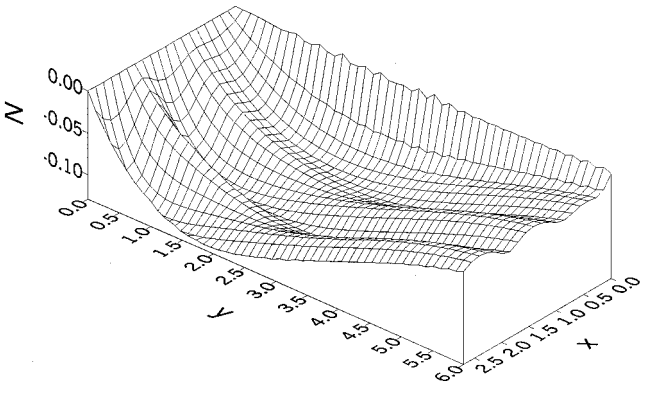

Fig. 12 Microrotation profiles of N ($\tau = 20, \alpha = 0.005, R = 5, \lambda = 5$, and $B = 1$).

Eq. (21) that in Fig. 10 the value of velocity gradient $\partial v / \partial y$ becomes a constant (i.e., $-2xU_w' / U_w$) far away from the wavy surface (i.e., $y \rightarrow \infty$).

Conclusions

A simple transposition theorem and the spline alternating-direction method have been used to study the forced convection flow and heat transfer along a wavy surface in micropolar fluids. The numerical results indicated that transient local skin-friction coefficient and the transient local and averaged heat-transfer rates decrease with time and that they all have a frequency equal to the frequency of the wavy surface. Moreover, as the values of the wavy length x and wavy amplitude α increase, the amplitudes of the skin-friction coefficient and the local Nusselt number tend to increase.

The crests and troughs of the transient local skin-friction coefficient and the transient local Nusselt number are shifted slightly upstream of the crests and troughs of the wavy surface. However, the crests and troughs of the transient total Nusselt number are shifted slightly downstream of the crests and troughs of the wavy surface. As the vortex viscosity parameter R increases, the transient heat-transfer rate decreases, but the transient skin friction increases. Furthermore, the transient heat-transfer rate of a micropolar fluid is smaller than that of a Newtonian fluid everywhere, but the transient skin friction of a micropolar fluid is larger than that of a Newtonian fluid near the leading edge.

References

[1] Eringen, A. C., "Theory of Micropolar Fluids," *Journal of Mathematical Mechanics*, Vol. 16, No. 1, 1966, pp. 1–16.

[2] Eringen, A. C., "Theory of Thermomicro Fluids," *Journal of Mathematical Analysis and Application*, Vol. 38, No. 9, 1972, pp. 480–490.

[3] Ariman, T., Turk, M. A., and Sylvester, N. D., "Microcontinuum Fluid Mechanics—A Review," *International Journal of Engineering Science*, Vol. 11, No. 8, 1973, pp. 905–930.

[4] Ariman, T., Turk, M. A., and Sylvester, N. D., "Applications of Microcontinuum Fluid Mechanics," *International Journal of Engineering Science*, Vol. 12, No. 4, 1974, pp. 273–293.

[5] Ahmadi, G., "Self-Similar Solution of Incompressible Micro-Polar Boundary Layer Flow over a Semi-Infinite Plate," *International Journal of Engineering Science*, Vol. 14, No. 7, 1976, pp. 639–646.

[6] Gorla, R. S. R., Pender, R., and Eppich, J., "Heat Transfer in Micro-Polar Boundary Layer Flow over a Flat Plate," *International Journal of Engineering Science*, Vol. 21, No. 7, 1983, pp. 791–798.

[7] Agarwal, Vijendra K., "Convective Heat Losses in Plat-Plate Collectors," *International Journal of Energy Research*, Vol. 8, No. 3, 1984, pp. 297–301.

[8] Lien, F. S., Chen, C. K., and Cleaver, J. W., "Analysis of Natural Convection Flow of Micropolar Fluid about a Sphere with Blowing and Suction," *Journal of Heat Transfer*, Vol. 108, No. 4, 1986, pp. 967–970.

[9] Lien, F. S., Chen, T. M., and Chen, C. K., "Analysis of a Free-Convection Micropolar Boundary Layer About a Horizontal Permeable Cylinder at a Nonuniform Thermal Condition," *Journal of Heat Transfer*, Vol. 112, No. 2, 1990, pp. 504–506.

[10] Yao, L. S., "Natural Convection Along a Vertical Wavy Surface," *Journal of Heat Transfer*, Vol. 105, No. 3, 1983, pp. 464–468.

[11] Chiu, C.-P., and Chou, H.-M., "Transient Analysis of Natural Convection Along a Vertical Wavy Surface in Micropolar Fluids," *International Journal of Engineering Science*, Vol. 32. No. 1, 1994, pp. 19–33.

[12] Takhar, H. S., Agarwal, R. S., Bhargava, R., and Jain, S., "Mixed Convection Flow of a Micropolar Fluid over a Stretching Sheet," *Heat and Mass Transfer*, Vol. 34, No. 2/3, 1998, pp. 213–219.

[13] Yao, L. S., "A Note on Prandtl's Transposition Theorem," *Journal of Heat Transfer*, Vol. 110, No. 2, 1988, pp. 503–507.

[14] Moulic, S. G., and Yao, L. S., "Mixed Convection Along a Vertical Wavy Surface," *Journal of Heat Transfer*, Vol. 111, No. 4, 1989, pp. 974–978.

[15] Rubin, S. G., and Graves, R. A., "Viscous Flow Solution with a Cubic Spline Approximation," *Computers and Fluids Journal*, Vol. 1, No. 5, 1975, pp. 1–36.

[16] Char, M. I., and Chen, C. K., "Temperature Field in Non-Newtonian Flow over a Stretching Plate with Variable Heat Flux," *International Journal of Heat and Mass Transfer*, Vol. 31, No. 5, 1988, pp. 917–921.

[17] Wang, P., and Kahawita, R., "Numerical Interration of Spatial Differential Equations Using Cubic Spline," *International Journal of Computer Mathematics*, Vol. 13, No. 3, 1983, pp. 271–286.